Noname manuscript No.
(will be inserted by the editor)

The Reaction Mass Biped: Geometric Mechanics and Control

Avinash Siravuru · Sasi P. Viswanathan · Koushil Sreenath · Amit K. Sanyal

the date of receipt and acceptance should be inserted later

Abstract Inverted Pendulum based reduced order models offer many valuable insights into the much harder problem of bipedal locomotion. While they help in understanding leg behavior during walking, they fail to capture the natural balancing ability of humans that stems from the variable rotational inertia on the torso. In an attempt to overcome this limitation, the proposed work introduces a Reaction Mass Biped (RMB). It is a generalization of the previously introduced *Reaction Mass Pendulum (RMP)*, which is a multi-body inverted pendulum model with an extensible leg and a variable rotational inertia torso. The dynamical model for the RMB is hybrid in nature, with the roles of stance leg and swing leg switching after each cycle. It is derived using a variational mechanics approach, and is therefore coordinate-free. The RMB model has thirteen degrees of freedom, all of which are considered to be actuated. A set of desired state trajectories that can enable bipedal walking in straight and curved paths are generated. A control scheme is then designed for asymptotically tracking this set of trajectories with an almost global domain-of-attraction. Numerical simulation results confirm the stability of this tracking control scheme for different walking paths of the RMB. Additionally, a discrete dynamical model is also provided along-with an appropriate Geometric Variational Integrator (GVI). In contrast to non-variational integrators, GVIs can better preserve energy terms for conservative mechanical systems and stability properties (achieved through energy-like lyapunov functions) for actuated systems.

A. Siravuru and K. Sreenath are with the Department of Mechanical Engineering, Carnegie Mellon University, Pittsburgh, PA 15213, USA asiravur@andrew.cmu.edu, koushils@cmu.edu · S. Viswanthan and A. K. Sanyal are with the Department of Mechanical and Aerospace Engineering, Syracuse University, Syracuse, NY 13244, USA {sviswana,aksanyal}@syr.edu. Preliminary results of this work were reported in [30].

1 Introduction

1.1 Background

Reduced-order models that are typically used for humanoid gait generation include several versions of the inverted pendulum model, such as the 2D and 3D linear inverted pendulum models (LIPM) [14,13], the cart-table model [12], the variable impedance LIPM [31], the spring-loaded inverted pendulum (SLIP) [1,5], and the angular momentum pendulum model (AMPM) [17,18]. All these models (except [17,18]) have limited utility for rotational maneuvers as they represent the entire humanoid body only as a point mass and do not characterize the significant rotational inertia of the torso. Neglecting it causes the angular momentum of the system about its CoM to be zero and the ground reaction force (GRF) to be directed along the lean line. It has been reported that during human gait, even at normal speed, the GRF diverges from the lean line [4] and this may be important for maintaining balance. The Reaction Mass Pendulum (RMP) model was introduced in [19] as a three-dimensional inverted pendulum model with variable inertia, which could be used as a reduced-order model for humanoid motion that accounted for the variable inertia and angular momentum of a humanoid body. This model consists of an extensible "leg" pinned to the ground along with a variable inertia "torso".

In order to model bipedal spatial locomotion, an extension of the Reaction Mass Pendulum (RMP) model developed in [19,4,26] is considered here. This extension adds a swing leg to the RMP model and it is termed the Reaction Mass Biped (RMB). The dynamics of this biped model is necessarily hybrid involving continuous-time stance dynamics with one foot on the ground and discrete-time impact dynamics when the swing foot hits the ground. Moreover, while most 3D models of bipedal robots model the rotational degrees of freedom through local coordinates such as Euler angles or quaternions, we consider a coordinate-free approach using rotation matrices. The dynamics are developed directly through application of the Lagrange-d'Alembert principle, by considering variations on the configuration manifolds. This leads to the development of a coordinate-free dynamical model that is valid globally and is free of singularities. Furthermore, these coordinate-free dynamics are discretized as well, yielding a structure preserving discrete-time stance dynamics. Using these discrete-time equations of motion a geometric variational integrator is developed to accurately integrate the system's dynamics.

On the control side, there is significant work in the formal stabilization of 3D walking using techniques based on controlled symmetries and Routhian reduction [7,6,29], and on hybrid zero dynamics [9,8]. These methods have been extended to yaw steering of 3D robots [28]. The present paper develops a geometric controller with a large domain of attraction.

1.2 Contributions

The main contributions of this paper with respect to prior work are listed below.

- A novel reduced order model, called Reaction Mass Biped, is proposed. Unlike many other popular models like LIPM, SLIP, etc., the RMB explicitly considers a variable inertia torso and models leg inertia.
- A Hybrid Geometric Model is developed using variational principles directly on the configuration manifold of the robot. The dynamics are said to be coordinate-free and have no singularity issues.
- A discrete mechanical model of the RMB is also developed along with a Geometric Variation Integrator (GVI).
- Assuming full actuation, a geometric trajectory tracking controller is developed for walking and turning with almost-global stability properties.

1.3 Organization

This paper is organized as follows: Section 2 describes the hybrid dynamical system model of the RMB. Section 3 develops a discrete mechanics model of the RMB, which is subsequently used to develop a structure-preserving geometric variational integrator. Section 4 develops motion primitives for walking alongwith a tracking controller to achieve the desired trajectories. Section 5 provides simulation results and discussions on the RMB walking along straight and curved paths. Finally, Section 6 provides concluding remarks.

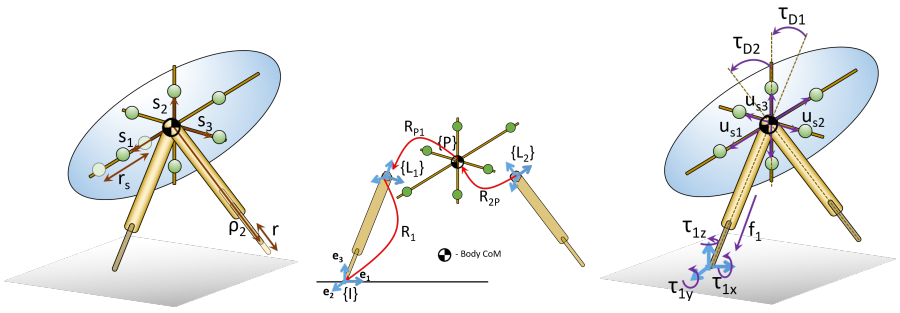

(a) RMB Model (b) Rotations (c) Actuation

Fig. 1: A schematic of the RMB model.

2 Mathematical Model

2.1 Physical description of the RMB Model

As shown in Fig.1(a), RMB consists of two extensible legs whose lengths are ρ_1 and ρ_2 as measured from the RMB CoM. The CoM of both the legs is assumed to coincide with the RMB CoM. Moreover,for some nominal length ρ_0, the moment of inertia for the legs is given by J_{L0}. The legs can extend up to a max distance r from ρ_0. The torso is made up of three pairs(depicted in green) of reaction masses s_1,s_2,s_3,respectively. Each pair is arranged along an orthogonal axis e_i of the torso's body-fixed frame. With one each on either side of the RMB CoM , they are constrained to move equidistantly so that the torso CoM always coincides with the RMB CoM. In Fig. 1(b), the frames of reference used in this study are depicted and they are defined in Table 1. We assume full actuation for the RMB model, as shown in Fig. 1(c). τ_1 rotates the ankle joint at the stance foot along pitch, roll and yaw directions w.r.t. the inertial frame $\{I\}$. f_1 is the force used to extend the telescopic stance leg. $\tau_{D1} \in \mathbb{R}^3$ rotates torso frame $\{P\}$ w.r.t the stance leg frame $\{L_1\}$. Similarly, $\tau_{D2} \in \mathbb{R}^3$ rotates swing leg frame $\{L_2\}$ w.r.t the torso frame $\{P\}$. Finally, $u_s \in \mathbb{R}^3$ actuates the reaction masses pairs on the torso. It is the motion of these point-masses that induces variability into the torso's inertia.

2.2 Stance Dynamics (or) Fixed-base Robot Model

We develop a coordinate-free dynamic model for the stance phase of the Reaction Mass Biped, as shown in Fig. 1(a), by using rotation matrices to represent the attitudes of the two legs, R_1, R_2, and the torso, R_P, along with scalars ρ_1, ρ_2 to represent the length of the two legs, and s_i to represent the position of the i^{th} pair of reaction masses. Note that, there are three pairs of reaction-masses, all of which are mutually orthogonal. During the stance phase, the stance-leg is assumed to be pinned to the ground. The configuration manifold of the system is then given by $\mathcal{Q}_s = C \times SO(3) \times SO(3) \times SO(3) \times S \times C$, with $\rho_1, \rho_2 \in C = [0, r]$, $R_1, R_P, R_2 \in SO(3)$, $s = \begin{bmatrix} s_1 & s_2 & s_3 \end{bmatrix}^T \in S = [0, r_s] \times [0, r_s] \times [0, r_s]$. The symbols used in this paper are tabulated in Table 1.

We have the following kinematic relations in the system, $\dot{R}_1 = R_1 \Omega_1^\times$, $\dot{R}_{P1} = R_{P1} \Omega_{P1}^\times$, $\dot{R}_P = R_P \Omega_P^\times$, $\dot{R}_{2P} = R_{2P} \Omega_{2P}^\times$, $\dot{R}_2 = R_2 \Omega_2^\times$, where, $\Omega_1, \Omega_2, \Omega_P$ are the respective body angular velocities, and are related by

$$\Omega_P = \Omega_{P1} + R_{P1}^{\mathrm{T}} \Omega_1, \quad \text{where,} \quad R_{P1} = R_1^{\mathrm{T}} R_P, \tag{1}$$

$$\Omega_2 = \Omega_{2P} + R_{2P}^{\mathrm{T}} \Omega_P, \quad \text{where,} \quad R_{2P} = R_P^{\mathrm{T}} R_2. \tag{2}$$

Here, the $(.)^\times$ is called the hat operator and it is used to map angular velocities from $\mathbb{R}^3$ to $\mathfrak{so}(3)$ (the Lie algebra of $\mathbb{SO}(3)$). Next, we derive an expression for the kinetic energy of the system, $\mathcal{T}_s : T\mathcal{Q}_s \to \mathbb{R}$. We do this

by first finding the position of the center-of-mass (COM) of the stance leg, b, and the positions of the reaction mass pairs, $p_{i\pm}$, in the inertial frame $\{I\}$ as follows,

$$b = \rho_1 R_1 e_3, \quad p_{i\pm} = b \pm s_i R_P e_i.$$

The dot product of their velocities can then be respectively computed as,

$$||\dot{b}||^2 = \dot{\rho}_1^2 - \rho_1^2 \Omega_1^T (e_3^\times)^2 \Omega_1 \tag{3}$$

$$||\dot{p}_{i+}||^2 + ||\dot{p}_{i-}||^2 = 2\left(||\dot{b}||^2 + \dot{s}_i^2 - s_i^2 \Omega_P (e_i^\times)^2 \Omega_P\right), \tag{4}$$

where $(\cdot)^\times : \mathbb{R}^3 \to \mathfrak{so}(3)$ is the skew operator, defined such that $x^\times y = x \times y, \forall x, y \in \mathbb{R}^3$. The kinetic energy of the system is then given by $\mathcal{T}_s = T_1 + T_P + T_2$, where, T_1, T_2 are the kinetic energies of the two legs respectively, and T_P is the kinetic energy of the torso, computed as,

$$\begin{aligned}
T_1 &= \frac{1}{2} m_L ||\dot{b}||^2 + \frac{1}{2} \Omega_1^T J_{L_0} \Omega_1, \\
T_P &= \frac{1}{2} m_P \left(\sum_{i=1}^{3} ||\dot{p}_{i+}||^2 + ||\dot{p}_{i-}||^2 \right) + \frac{1}{2} \Omega_P^T J_{P_0} \Omega_P, \\
T_2 &= \frac{1}{2} m_L ||\dot{b}||^2 + \frac{1}{2} \Omega_2^T J_{L_0} \Omega_2.
\end{aligned}$$

Thus, the total kinetic energy of the system is,

$$\mathcal{T}_s = \frac{1}{2} m \dot{\rho}_1^2 + \sum_{i=1}^{3} m_P \dot{s}_i^2 + \frac{1}{2} \Omega_1^T J_1(\rho_1) \Omega_1 + \frac{1}{2} \Omega_P^T J_P(s) \Omega_P + \frac{1}{2} \Omega_2^T J_{L_0} \Omega_2, \tag{5}$$

where,

$$\begin{aligned}
J_1(\rho_1) &= J_{L_0} + K_1(\rho_1), \qquad K_1(\rho_1) = -m\rho_1^2 (e_3^\times)^2, \qquad m = 2m_L + 6m_P, \\
J_P(s) &= J_{P_0} + K_P(s), \quad K_P(s) = -2 \textstyle\sum_{i=1}^{3} m_P s_i^2 (e_i^\times)^2.
\end{aligned}$$

Remark 1 Note that, the length of the swing leg, ρ_2 does not appear in the kinetic energy of the system, and as we will consequently see, it will not appear in the dynamics either. This is because of representing COM of the swing leg at the hip. Moving COM location to half-way along the leg will ensure the swing leg length velocity appears in the kinetic energy, thereby introducing an additional dynamical equation for ρ_2. The dynamical model and the controller developed here can easily be extended to incorporate a variable swing leg length, at the cost of adding another degree of freedom and some complexity to the dynamics. Here we treat the simpler case by assuming the swing leg length to be constant. The swing leg's rotation does appear in the kinetic energy through Ω_2.

Having developed an expression for the kinetic energy, we next compute the Potential Energy, $\mathcal{U}_s : \mathcal{Q}_s \to \mathbb{R}$, as,

$$\mathcal{U}_s = -mg\rho_1 R_1^T e_3 \cdot e_3. \tag{6}$$

$m_L \in \mathbb{R}$	Mass of either Leg at Hip Joint
$m_P \in \mathbb{R}$	Mass of Reaction masses
$m \in \mathbb{R}$	Mass of the entire system
$J_{L_0} \in \mathbb{R}^{3\times3}$	Inertia matrix of either leg with respect to the body-fixed frame when leg length is its nominal value ρ_0
$J_{P_0} \in \mathbb{R}^{3\times3}$	Inertia matrix of the torso with respect to the body-fixed frame
$\{I\}$	Inertial frame at the stance foot
$\{L_1\}$	Body frame of the stance leg at the hip joint
$\{P\}$	Body frame of the torso at the hip joint
$\{L_2\}$	Body frame of the swing leg at the hip joint
$\rho_1 \in C$	Distance between CoM of the stance leg and its ankle
$\rho_0 \in C$	Constant distance between CoM of the swing leg and the hip joint
$R_1 \in SO(3)$	Rotation matrix of the stance leg from the body-fixed frame to the inertial frame {I}
$R_P \in SO(3)$	Rotation matrix of the torso from the body-fixed frame to the inertial frame {I}
$R_2 \in SO(3)$	Rotation matrix of the swing leg from the body-fixed frame to the inertial frame {I}
$R_{P1} \in SO(3)$	Rotation matrix of the torso from the body-fixed frame {P} to the stance leg body-fixed frame $\{L_1\}$
$R_{2P} \in SO(3)$	Rotation matrix of the swing leg from the body-fixed frame $\{L2\}$ to the torso body-fixed frame {P}
$\Omega_1 \in \mathbb{R}^3$	Angular velocity of the stance leg in the body-fixed frame
$\Omega_2 \in \mathbb{R}^3$	Angular velocity of the swing leg in the body-fixed frame
$\Omega_P \in \mathbb{R}^3$	Angular velocity of the torso in the body-fixed frame
$s_i \in S$	Position of the i'th reaction mass
$e_3 \in \mathbb{R}^3$	Standard unit vector along the gravity direction (downward) in the inertial frame

Table 1: Enumeration of the symbolic notation used in the paper.

Note that the negative sign arises due to our convention of e_3 being along the direction of uniform gravity.

The Lagrangian of the system $\mathcal{L}_s : T\mathcal{Q}_s \to \mathbb{R}$ is then given by $\mathcal{L}_s = \mathcal{T}_s - \mathcal{U}_s$. The equations of motion can then be computed through the Lagrange-d'Alembert principle by writing the variation of the action integral as,

$$\int \left(\delta\mathcal{L}_s + \eta_1 \cdot \tau_1 + \delta\rho_1 f_1 + \eta_{P1} \cdot \tau_{D_1} + \sum_{i=1}^{3} \delta s_i u_{s_i} + \eta_{P2} \cdot \tau_{D_2} \right), \tag{7}$$

where the first term in the integral represents the variation of the Lagrangian, computed using the following variations on SO(3),

$$\delta R_1 = R_1 \eta_1^{\times},\ \eta_1 \in \mathbb{R}^3,\quad \delta\Omega_1 = \Omega_1^{\times}\eta_1 + \dot{\eta}_1, \tag{8}$$

$$\delta R_P = R_P \eta_P^{\times},\ \eta_P \in \mathbb{R}^3,\quad \delta\Omega_P = \Omega_P^{\times}\eta_P + \dot{\eta}_P, \tag{9}$$

$$\delta R_2 = R_2 \eta_2^{\times},\ \eta_2 \in \mathbb{R}^3,\quad \delta\Omega_2 = \Omega_2^{\times}\eta_2 + \dot{\eta}_2, \tag{10}$$

and, all the other subsequent terms in the integral representing the infinitesimal virtual work, where,

$$\eta_{P1} = \eta_P - R_P^T R_1 \eta_1, \qquad \eta_{P2} = \eta_2 - R_2^T R_P \eta_P.$$

For more details and illustrations of the actuators, please refer to Fig. 1(c). The dynamical equations of motion can then be obtained by setting the above

integral to zero for all possible variations, resulting in,

$$
\begin{aligned}
m\ddot{\rho}_1 &= -m\rho_1 \Omega_1^T (e_3^\times)^2 \Omega_1 + mge_3^T R_1^T e_3 + f_1, && (11)\\
J_1(\rho_1)\dot{\Omega}_1 &= -\Omega_1 \times J_1(\rho_1)\Omega_1 + 2m\rho_1\dot{\rho}_1(e_3^\times)^2\Omega_1 \\
&\quad + \ mg\rho_1 e_3^\times R_1^T e_3 + \tau_1 - R_1^T R_P \tau_{D_1}, && (12)\\
J_P(s)\dot{\Omega}_P &= -\Omega_P \times J_P(s)\Omega_P - N(s,\dot{s})\Omega_P \\
&\quad + \ \tau_{D_1} - R_P^T R_2 \tau_{D_2}, && (13)\\
2m_P\ddot{s} &= \ -L(s,\Omega_P) + u_s, && (14)\\
J_{L_0}\dot{\Omega}_2 &= -\Omega_2 \times J_{L_0}\Omega_2 + \tau_{D_2}, && (15)
\end{aligned}
$$

where, $N(s,\dot{s}) = \dfrac{\mathrm{d}}{\mathrm{d}t}K_P(s) = 4m_P \,\mathrm{diag}\,\{s_2\dot{s}_2 + s_3\dot{s}_3, s_1\dot{s}_1 + s_3\dot{s}_3, s_1\dot{s}_1 + s_2\dot{s}_2\}$,

$$
\text{and, } L(s,\Omega_P) = \frac{\partial}{\partial s}(\frac{1}{2}\,\Omega_P^{\mathrm{T}}\,K_P\,\Omega_P) = 2m_P \begin{bmatrix} s_1(\Omega_{P_2}^2 + \Omega_{P_3}^2) \\ s_2(\Omega_{P_3}^2 + \Omega_{P_1}^2) \\ s_3(\Omega_{P_1}^2 + \Omega_{P_2}^2) \end{bmatrix}.
$$

We can rewrite the above dynamical equations in a matrix form (useful for the impact model) by defining $\boldsymbol{q_s} = \big(\rho_1, R_1, R_P, s, R_2\big)$, and $\boldsymbol{\omega_s} = \big[\dot{\rho}_1 \ \Omega_1 \ \Omega_P \ \dot{s} \ \Omega_2\big]^T$. Thus, using $\boldsymbol{q_s}, \boldsymbol{\omega_s}$, the equations of motion can be rewritten as

$$
\boldsymbol{D_s}(\boldsymbol{q_s})\dot{\boldsymbol{\omega}}_s = \boldsymbol{H_s}(\boldsymbol{q_s}, \boldsymbol{\omega_s}) + \boldsymbol{B_s}\boldsymbol{u_s},
$$

where, $\boldsymbol{D_s}(\boldsymbol{q_s}) = diag\,(m, J_1(\rho_1), J_P(s), 2m_P I, J_{L_0})$, and

$$
\boldsymbol{H_s}(\boldsymbol{q_s}, \boldsymbol{\omega_s}) = \begin{bmatrix} -m\rho_1\Omega_1^T(e_3^\times)^2\Omega_1 + mge_3^T R_1^T e_3 \\ -\Omega_1 \times J_1(\rho_1)\Omega_1 + 2m\rho_1\dot{\rho}_1(e_3^\times)^2\Omega_1 + mg\rho_1 e_3^\times R_1^T e_3 \\ -\Omega_P \times J_P(s)\Omega_P + 4\sum_{i=1}^{3} m_P s_i \dot{s}_i (e_i^\times)^2 \Omega_P \\ -L(s,\Omega_P) \\ -\Omega_2 \times J_{L_0}\Omega_2 \end{bmatrix},
$$

$$
\boldsymbol{B_s}(\boldsymbol{q_s}) = \begin{bmatrix} I & 0 & 0 & 0 & 0 \\ 0 & I & -R_1^T R_P & 0 & 0 \\ 0 & 0 & I & 0 & -R_P^T R_2 \\ 0 & 0 & 0 & I & 0 \\ 0 & 0 & 0 & 0 & I \end{bmatrix}, \boldsymbol{u_s} = \begin{bmatrix} f_1 \\ \tau_1 \\ \tau_{D1} \\ u_s \\ \tau_{D2} \end{bmatrix}.
$$

Remark 2 Note that the stance dynamics of the Reaction Mass Biped is fully actuated due to the ankle torque τ_1 at the stance foot.

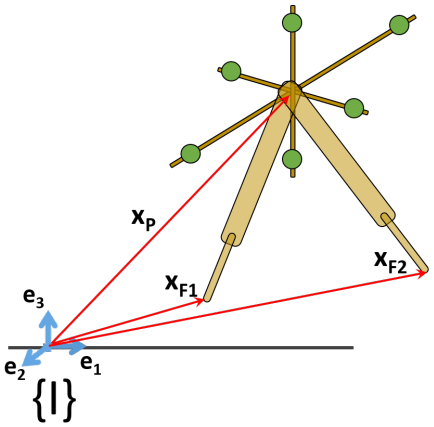

Fig. 2: Reaction Mass Biped Model for the Extended Dynamics or the Floating base case. Here, x_P is the hip position while x_{F1}, x_{F2} are the stance and swing leg positions, respectively. In the flight phase, we assume that both $\rho_1 = \rho_2 = \rho_0$ i.e., both legs don't extend but only rotate.

2.3 Extended Dynamics or Floating-base Robot Model

Having derived the stance dynamics of the Reaction Mass Biped system, where the stance leg is pinned to the ground, we now develop the extended model, where the foot is no longer pinned to the ground. This model is required to formulate the discrete-time impact model that captures the dynamics of swing foot impact with the ground. The extended model is illustrated in Figure 2, and has the configuration manifold $\mathcal{Q}_e = \mathbb{R}^3 \times SO(3) \times SO(3) \times S \times SO(3)$. The kinetic and potential energies, $\mathcal{T}_e : T\mathcal{Q}_e \to \mathbb{R}, \mathcal{U}_e : Q_e \to \mathbb{R}$ can be derived in a similar manner as in the stance dynamics, resulting in,

$$\begin{aligned}\mathcal{T}_e &= \frac{1}{2} m \dot{x}_P \cdot \dot{x}_P + \sum_{i=1}^{3} m_P \dot{s}_i^2 + \frac{1}{2} \Omega_1^T J_{L_0} \Omega_1 \\ &\quad + \frac{1}{2} \Omega_P^T J_P(s) \Omega_P + \frac{1}{2} \Omega_2^T J_{L_0} \Omega_2, \qquad (16)\\ \mathcal{U}_e &= -mg x_P \cdot e_3. \qquad (17)\end{aligned}$$

The dynamics of motion can be obtained through application of the Lagrange-d'Alembert principle as outlined earlier. We will directly write this in matrix form by first defining, $\boldsymbol{q}_e = \big(R_1, R_P, s, R_2, x_P\big)$, and $\boldsymbol{\omega}_e = \big[\Omega_1 \ \Omega_P \ \dot{s} \ \Omega_2 \ \dot{x}_P\big]^T$, where x_P is the position of the hip in the inertial frame. We then have,

$$\boldsymbol{D}_e(\boldsymbol{q}_e)\dot{\boldsymbol{\omega}}_e = \boldsymbol{H}_e(\boldsymbol{q}_e, \boldsymbol{\omega}_e) + \boldsymbol{B}_e(\boldsymbol{q}_e)\boldsymbol{u}_e,$$

where, $\boldsymbol{D}_e(\boldsymbol{q}_e) = diag\left(J_{L_0}, J_P(s), 2m_P I, J_{L_0}, m\right)$,

$$\boldsymbol{H}_e(\boldsymbol{q}_e, \boldsymbol{\omega}_e) = \begin{bmatrix} -\Omega_1 \times J_{L_0}\Omega_1 \\ -\Omega_P \times J_P(s)\Omega_P + 4\sum_{i=1}^{3} m_P s_i \dot{s}_i (e_i^{\times})^2 \Omega_P \\ -L(s, \Omega_P) \\ -\Omega_2 \times J_{L_0}\Omega_2 \\ mge_3 \end{bmatrix}, \tag{18}$$

$$\boldsymbol{B}_e(\boldsymbol{q}_e) = \begin{bmatrix} -R_1^T R_P & 0 & 0 \\ I & 0 & -R_P^T R_2 \\ 0 & I & 0 \\ 0 & 0 & I \\ 0 & 0 & 0 \end{bmatrix}, \quad \boldsymbol{u}_e = \begin{bmatrix} \tau_{D1} \\ u_s \\ \tau_{D2} \end{bmatrix}. \tag{19}$$

Remark 3 Note that the extended dynamical model of the reaction mass biped is under-actuated. This is in contrast to the stance dynamical model, which is fully actuated.

2.4 Impact Model

We will next develop the discrete-time impact model that captures the impact of the swing foot with the ground. The impact model results in an instantaneous change in the joint velocities of the system. In order to capture this, we will first need to map the stance coordinates to the extended coordinates, perform the impact in the extended coordinates, map the extended coordinates to the stance coordinates while accounting for the relabeling that occurs as the old swing leg becomes the new stance leg.

First, to map the stance coordinates to the extended coordinates, we need to find $x_P, \dot{x}_P$ in terms of the stance coordinates. Since the stance foot is on the ground, $x_P = \rho_1 R_1 e_3$. From this we obtain, $\dot{x}_P = \dot{\rho}_1 R_1 e_3 + \rho_1 R_1 \Omega_1^{\times} e_3$. We will write this as the following map,

$$\boldsymbol{q}_e = \Upsilon^{\boldsymbol{q}}_{s\to e}(\boldsymbol{q}_s), \quad \boldsymbol{\omega}_e = \Upsilon^{\boldsymbol{\omega}}_{s\to e}(\boldsymbol{\omega}_s).$$

For later use, we will denote the map from the extended coordinates to the stance coordinates (assuming the first leg's foot is in contact with the ground) as,

$$\boldsymbol{q}_s = \Upsilon^{\boldsymbol{q}}_{e\to s}(\boldsymbol{q}_e), \quad \boldsymbol{\omega}_s = \Upsilon^{\boldsymbol{\omega}}_{e\to s}(\boldsymbol{\omega}_e).$$

This map essentially computes ρ_1 from x_P as, $\rho_1 = ||x_P||$.

Next we model the impact map. By considering $(\boldsymbol{q}_e^-, \boldsymbol{\omega}_e^-)$ to be the state prior to impact, and $(\boldsymbol{q}_e^+, \boldsymbol{\omega}_e^+)$ to be the state post impact, and F_{ext} representing the external force, we have the following relation from [10],

$$\boldsymbol{D}(\boldsymbol{q}_e^+)\boldsymbol{\omega}_e^+ - \boldsymbol{D}(\boldsymbol{q}_e^-)\boldsymbol{\omega}_e^- = F_{ext}.$$

Further, the swing foot position and velocity are given as,

$$x_{F_2} = x_P + \rho_2^{td} R_2 e_3, \quad \dot{x}_{F_2} = \dot{x}_P - \rho_2^{td} R_2 (e_3)^{\times} \Omega_2,$$

where ρ_2^{td} is the value of ρ_2 at touchdown (note that ρ_2^{td} is a constant and has no dynamics since ρ_2 can instantaneously change.) We require the post impact swing foot velocity $\dot{x}_{F_2}^+ = 0$, since this foot now becomes the new stance foot. This can be expressed as $A\boldsymbol{\omega}_e^+ = 0$, where,

$$A = \begin{bmatrix} 0\ 0\ 0\ -\rho_2^{td} R_2^+ (e_3)^\times \ I \end{bmatrix}.$$

Further, denoting I_R as the impact force at the swing foot, we have $F_{ext} = A^T I_R$. The above equations can then be expressed in matrix form to solve for $\boldsymbol{\omega}_e^+$ and I_R,

$$\begin{bmatrix} \boldsymbol{\omega}_e^+ \\ I_R \end{bmatrix} = \begin{bmatrix} \boldsymbol{D}_e(\boldsymbol{q}_e^+) & -A^T \\ A & 0 \end{bmatrix}^{-1} \begin{bmatrix} -\boldsymbol{D}_e(\boldsymbol{q}_e^-)\boldsymbol{\omega}_e^- \\ 0 \end{bmatrix}. \tag{20}$$

We can then define a map Γ such that $\boldsymbol{\omega}_e^+ = \Gamma(\boldsymbol{\omega}_e^-)$.

The impact map can then be defined by the map $\Delta_{s\to s} : \mathcal{S} \to TQ$, where $\mathcal{S} = \{x_s \in TQ_s \mid (\rho_2 R_2 e_3 - \rho_1 R_1 e_3) \cdot e_3 = 0\}$ is the switching surface representing the contact of the swing leg toe with the ground. We have,

$$\Delta_{s\to s} := \begin{bmatrix} \Delta_{s\to s}^{\boldsymbol{q}} \\ \Delta_{s\to s}^{\boldsymbol{\omega}} \end{bmatrix},$$

where, the components $\Delta_{s\to s}^{\boldsymbol{q}}$ and $\Delta_{s\to s}^{\boldsymbol{\omega}}$ define the transition maps for the configuration variables and their velocities, respectively. These are obtained from the above equations as follows:

$$\begin{aligned} \Delta_{s\to s}^{\boldsymbol{q}} &:= \Upsilon_{e\to s}^{\boldsymbol{q}} \circ \mathcal{R} \circ \Upsilon_{s\to e}^{\boldsymbol{q}}, \\ \Delta_{s\to s}^{\boldsymbol{\omega}} &:= \Upsilon_{e\to s}^{\boldsymbol{\omega}} \circ \mathcal{R} \circ \Gamma \circ \Upsilon_{s\to e}^{\boldsymbol{\omega}}, \end{aligned}$$

where $\mathcal{R}$ represents a coordinate relabeling transformation such that the old swing leg is labeled as the new stance leg and vice-versa.

2.5 Hybrid System Model

The hybrid model for walking is based on the stance dynamics and the impact model developed in the previous sections, and can be represented as follows:

$$\Sigma : \begin{cases} \boldsymbol{D}_s \dot{\boldsymbol{\omega}}_s = \boldsymbol{H}_s(\boldsymbol{q}_s, \boldsymbol{\omega}_s) + \boldsymbol{B}_s(\boldsymbol{q}_s)\boldsymbol{u}_s, & (\boldsymbol{q}_s^-, \boldsymbol{\omega}_s^-) \notin \mathcal{S}, \\ (\boldsymbol{q}_s^+, \boldsymbol{\omega}_s^+) = \Delta_{s\to s}(\boldsymbol{q}_s^-, \boldsymbol{\omega}_s^-), & (\boldsymbol{q}_s^-, \boldsymbol{\omega}_s^-) \in \mathcal{S}. \end{cases}$$

3 Discrete Mechanics and Variational Integrator for RMB

In general, for hybrid dynamical models like the RMB, conventional numerical integrators, based on explicit Runge-Kutta method, are used for determining the system's flow based on the continuous-time Euler-Lagrange equations that were derived in Section 2. However, this procedure results in the loss of some fundamental geometric properties of the system such as, inherent manifold structure, symplecticity, and the momentum map. Special integrators exist to

either preserve manifold structure of the configuration space [11,16] or simplecticity [22,33]. Recently, Lee et al [21,20] integrated these two techniques and devised Geometric Variational Integrators (GVI) that are capable of preserving both geometry and structure of the discrete flow. In this section, we develop a discrete mechanics model of the RMB by taking variations of the corresponding discrete action sum. The resulting update rules form the discrete equations of motion and they used to construct a GVI for the RMB system.

3.1 Discrete Lagrangian

The Lagrangian is discretized with a fixed step size, $h \geq 0$, and the subscript k determines the value at any iteration, as $t_k = kh$. Therefore, the configuration manifold of the RMB at any time t_k is given as $\mathcal{Q}_s = C \times SO(3) \times SO(3) \times SO(3) \times S \times C$, with configuration variables $\rho_{1_k}, \rho_{2_k} \in C = [0, r]$, $R_{1_k}, R_{P_k}, R_{2_k} \in SO(3)$, $s_k = \begin{bmatrix} s_{1_k} & s_{2_k} & s_{3_k} \end{bmatrix}^T \in S$.

For the discrete-time kinematic relations, the linear velocity $\dot{x}_k$ at t_k can be approximated as shown

$$\dot{x}_k \approx \frac{\Delta x_k}{h} = \frac{x_{k+1} - x_k}{h}. \tag{21}$$

Similarly, from the rotational kinematic relations in Section 2, the discrete analogue of angular velocity is

$$F_k = e^{h\Omega_k^\times}, \text{ so that } R_{k+1} = R_k F_k. \tag{22}$$

Using (22) and (21), we get the following first order discrete equations for the RMB,

$$R_{1_{k+1}} = R_{1_k} F_{1_k},\ R_{P_{k+1}} = R_{P_k} F_{P_k},\ R_{2_{k+1}} = R_{2_k} F_{2_k}, \tag{23}$$

$$\rho_{1_{k+1}} = \rho_{1_k} + h\dot{\rho}_{1_k},\ s_{k+1} = s_k + h\dot{s}_k. \tag{24}$$

$F_{1_k} \in SO(3)$	Rotation matrix that shifts the stance leg from configuration R_{1_k} to $R_{1_{k+1}}$ during k^{th} time-step
$F_{P_k} \in SO(3)$	Rotation matrix that shifts the torso from configuration R_{P_k} to $R_{P_{k+1}}$ during k^{th} time-step
$F_{2_k} \in SO(3)$	Rotation matrix that shifts the swing leg from configuration R_{2_k} to $R_{2_{k+1}}$ during k^{th} time-step

Table 2: Notations used in the discrete mechanics of RMB

The symbols specific to the discrete mechanics are tabulated in Table 2. We derive the discrete versions of both kinetic ($\mathcal{T}_s$) and potential ($\mathcal{U}_s$) energies of the system next. The discrete version of potential energy $\mathcal{U}_{s_k} : \mathcal{Q}_s \to \mathbb{R}$ is given

as $\mathcal{U}_{s_k} = -mg\rho_{1_k} e_3^T R_{1_k}^T e_3$, and the kinetic energy, defined as $\mathcal{T}_{s_k} : T\mathcal{Q}_s \to \mathbb{R}$, is given as,

$$\mathcal{T}_{s_k} = \frac{1}{2}(m\dot{\rho}_{1_k}^2 + \sum_{i=1}^{3} m_P \dot{s}_{i_k}^2 + \Omega_{1_k}^T J_1(\rho_{1_k})\Omega_{1_k} + \Omega_{P_k}^T J_P(s_k)\Omega_{P_k} + \Omega_{2_k}^T J_{L_0}\Omega_{2_k}). \tag{25}$$

The discrete Lagrangian $\mathcal{L}_k$ approximates the path of least action, which is obtained by integrating the Lagrangian along the exact solution of the equations of motion for a single time step,

$$\mathcal{L}_k \approx \int_0^h L dt = L(\rho_{1_k}, s_k, \Omega_{1_k}, \Omega_{P_k}, \Omega_{2_k})h = \mathcal{T}_{s_k} - \mathcal{U}_{s_k}. \tag{26}$$

Substituting (25) in (26) gives

$$\mathcal{L}_k = \tfrac{h}{2}[\dot{\rho}_{1_k}\ \dot{s}_k\ \Omega_{1_k}\ \Omega_{P_k}\ \Omega_{2_k}]^T \begin{bmatrix} m & & & & & \\ & 2m_P I & & & & \\ & & J_1(\rho_{1_k}) & & & \\ & & & J_P(s_k) & & \\ & & & & J_{L_0} \end{bmatrix} \begin{bmatrix} \dot{\rho}_{1_k} \\ \dot{s}_k \\ \Omega_{1_k} \\ \Omega_{P_k} \\ \Omega_{2_k} \end{bmatrix} + hmg\rho_{1_k} e_3^T R_{1_k}^T e_3, \tag{27}$$

where $J_1(\rho_{1_k}) = J_{L_0} - m\rho_{1_k}^2 (e_3^\times)^2$, $J_P(s_k) = J_{P_0} - 2\sum_{i=1}^{3} m_P s_{i_k}^2 (e_i^\times)^2$. Similar to its continuous-time counterpart, the discrete-time version of the Lagrange-d'Alembert principle states that the action sum, which approximates the action integral, is invariant to the first order of all possible variations, as shown in (28). Integrators that maintain this invariance are called Variational Integrators. Additionally, if they also maintain the structure of the configuration manifold, they are called GVIs.

$$\delta\mathcal{S}_d = \sum_{k=0}^{N-1} \delta\mathcal{L}_k + \delta\mathcal{W}_k = 0, \quad \text{where} \quad N = \frac{t_F - t_0}{h}. \tag{28}$$

Here, t_0, t_F are the start and end times of the integration, respectively. To compute the above, we have to first determine the infinitesimal variations for R_k and Ω_k, as shown in [32],

$$\delta R_k = \lim_{\epsilon \to 0} R_k \exp(\epsilon \eta_k^\times) = R_k \eta_k^\times, \tag{29}$$

$$\delta F_k = h\delta\Omega_k^\times \exp(h\Omega_k^\times) = h\delta\Omega_k^\times F_k, \tag{30}$$

$$\implies \delta\Omega_k^\times = \frac{1}{h}\delta F_k F_k^T = \frac{1}{h}((F_k\eta_{k+1})^\times - \eta_k^\times),$$

$$\therefore \delta\Omega_k = \frac{1}{h}((F_k\eta_{k+1}) - \eta_k). \tag{31}$$

Additionally, the variations of $\dot{\rho}_{1_k}$ and $\dot{s}_k$ are,

$$\delta\dot{\rho_{1}}_k = \frac{\delta\rho_{1_{k+1}} - \delta\rho_{1_k}}{h},\ \delta\dot{s_k} = \frac{\delta s_{k+1} - \delta s_k}{h}. \tag{32}$$

The infinitesimal virtual work done and Lagrangian can be discretized using the discrete infinitesimal variations obtained above as follows:

$$\begin{aligned}
\delta\mathcal{W}_k &= h(f_{1_k}\delta\rho_{1_k} + u_{s_k}^T\delta s_k + \tau_{1_k}^T\eta_{1_k} + \tau_{D_{1_k}}^T\eta_{P1_k} + \tau_{D_{2_k}}^T\eta_{P2_k}),\\
\delta\mathcal{L}_k &= h[\dot{\rho}_{1_k}\ \dot{s}_k\ \Omega_{1_k}\ \Omega_{P_k}\ \Omega_{2_k}]^T
\begin{bmatrix} m & & & & \\ & 2m_PI & & & \\ & & J_1(\rho_{1_k}) & & \\ & & & J_P(s_k) & \\ & & & & J_{L_0} \end{bmatrix}
\begin{bmatrix} \delta\dot{\rho}_{1_k} \\ \delta\dot{s}_k \\ \delta\Omega_{1_k} \\ \delta\Omega_{P_k} \\ \delta\Omega_{2_k} \end{bmatrix}\\
&\quad -hm\rho_{1_k}\Omega_{1_k}^T(e_3^\times)^2\Omega_{1_k}\delta\rho_{1_k} - h2m_P\textstyle\sum_{i=1}^3 s_{i_k}\Omega_{P_k}^T(e_i^\times)^2\Omega_{P_k}\delta s_{i_k}\\
&\quad +hmg\delta\rho_{1_k}e_3^TR_{1_k}^Te_3 + hmg\rho_{1_k}e_3^T\delta R_{1_k}^Te_3.
\end{aligned} \tag{33}$$

Now, we map all the velocities to their corresponding momentum terms and continue the rest of this derivation in terms of the momenta. Let, $p_{\rho_{1_k}} = m\dot{\rho}_{1_k}$, $p_{s_k} = 2m_P\dot{s}_k$, $\Pi_{1_k} = J_1(\rho_{1_k})\Omega_{1_k}$, $\Pi_{P_k} = J_P(s_{P_k})\Omega_{P_k}$, and $\Pi_{2_k} = J_{L_0}\Omega_{2_k}$. Accordingly, the discrete action sum in (28) can be rewritten using (33) as,

$$\begin{aligned}
\delta\mathcal{S}_d &= \textstyle\sum_{k=0}^{N-1}[\Pi_{1_k}^T\delta\Omega_{1_k} + M_k^T\delta R_{1_k} + \Pi_{P_k}^T\delta\Omega_{P_k} + \Pi_{2_k}^T\delta\Omega_{2_k} +\\
&\quad p_{\rho_{1_k}}(\delta\rho_{1_{k+1}} - \delta\rho_{1_k}) - hm\rho_{1_k}\Omega_{1_k}^T(e_3^\times)^2\Omega_{1_k}\delta\rho_{1_k} + N_k\delta\rho_{1_k} +\\
&\quad \textstyle\sum_{i=1}^3 p_{s_{i_k}}(\delta s_{i_{k+1}} - \delta s_{i_k}) - h2m_Ps_{i_k}\Omega_{P_k}^T(e_i^\times)^2\Omega_{P_k}\delta s_{i_k} + \delta\mathcal{W}_k] = 0.
\end{aligned} \tag{34}$$

where, $M_k = \frac{\partial\mathcal{U}_{s_k}}{\partial R_{1_k}}$ and $N_k = \frac{\partial\mathcal{U}_{s_k}}{\partial\rho_{1_k}}$. We can substitute (33), and the variations (29),(31), and (32) in (34) to obtain the discrete action sum in terms of the variations $\delta\upsilon_k := [\eta_{1_k}\ \eta_{P_k}\ \eta_{2_k}\ \delta\rho_{1_k}\ \delta s_k]$. The fact that variations vanish at end points, i.e., $\delta\upsilon_k = 0$ if $k = \{0, N\}$, and an appropriate re-indexing of terms allows us to reformulate (34) as,

$$\begin{aligned}
&\sum_{k=1}^{N-1}[(F_{1_{k-1}}^T\Pi_{1_{k-1}} - \Pi_{1_k} + M_k^TR_{1_k} + h\tau_{1_k} - hR_{P1_k}\tau_{D1_k})^T\eta_{1_k}\\
&\qquad (F_{P_{k-1}}^T\Pi_{P_{k-1}} - \Pi_{P_k} + h\tau_{D1_k} - hR_{P2_k}\tau_{D2_k})^T\eta_{p_k} +\\
&\qquad (F_{2_{k-1}}^T\Pi_{2_{k-1}} - \Pi_{2_k} + h\tau_{D2_k})^T\eta_{2_k} +\\
&\quad (p_{\rho_{1_{k-1}}} - p_{\rho_{1_k}} - hm\rho_{1_k}\Omega_{1_k}^T(e_3^\times)^2\Omega_{1_k} + N_k + hf_{1_k})\delta\rho_{1_k} +\\
&\sum_{i=1}^3(p_{s_{i_{k-1}}} - p_{s_{i_k}} - h2m_Ps_{i_k}\Omega_{P_k}^T(e_i^\times)^2\Omega_{P_k} + hu_{i_k})\delta s_{i_k}] = 0.
\end{aligned} \tag{35}$$

Since (35) is true for any $\delta\upsilon_k$, we require that the expressions each of in the parentheses to be equal to zero. They are indeed the discrete-time equations of

motion for the RMB in terms of the momenta. Finally, we can map back from the momentum terms to the velocity terms to get the equations of motion in terms of the velocities as shown below:

$$J_{1_{k+1}}\Omega_{1_{k+1}} = F_{1_k}^T(J_{1_k}\Omega_{1_k}) + hmg\rho_{1_{k+1}}e_3^\times R_{1_{k+1}}^T e_3 + h\tau_{1_{k+1}} - \ hR_{P1_{k+1}}\tau_{D1_{k+1}} \tag{36}$$

$$J_{P_{k+1}}\Omega_{P_{k+1}} = F_{P_k}^T(J_{P_k}\Omega_{P_k}) + h\tau_{D1_{k+1}} - hR_{P2_{k+1}}\tau_{D2_{k+1}} \tag{37}$$

$$J_{L_0}\Omega_{2_{k+1}} = F_{2_k}^T(J_{L_0}\Omega_{2_k}) + h\tau_{D2_{k+1}} \tag{38}$$

$$m\dot{\rho}_{1_{k+1}} = m\dot{\rho}_{1_k} - hm\rho_{1_{k+1}}\Omega_{1_{k+1}}^T(e_3^\times)^2\Omega_{1_{k+1}} + hmge_3^T R_{1_{k+1}}^T e_3 + hf_{1_{k+1}} \tag{39}$$

$$2m_P\dot{s}_{k+1} = 2m_P\dot{s}_k - hL(s_{k+1}, \Omega_{P_{k+1}}) + hu_{k+1} \tag{40}$$

The discrete-time Lagrangian flow map takes us from $(\Omega_{1_k}\ \Omega_{P_k}\ \Omega_{2_k}\ \dot{\rho}_{1_k}\ \dot{s}_k) \mapsto (\Omega_{1_{k+1}}\ \Omega_{P_{k+1}}\ \Omega_{2_{k+1}}\ \dot{\rho}_{1_{k+1}}\ \dot{s}_{k+1})$, and this process is repeated for N steps. Note that, unlike in [21,20], this is an explicit method and doesn't require custom Rodrigues formula-based gradient descent methods, and is therefore faster.

3.2 Advantages of Geometric Variational Integrators are listed below.

1. GVIs preserve important mechanical properties like energy conservation (for conservative systems), momentum conservation (where there is symmetry), while ensuring that the dynamics evolves in the configuration manifold of the system.
2. They can be easily implemented in hardware and the equations are inherently discrete-time.
3. This structure preserving property is also useful when building controllers based on energy-like Lyapunov functions, as shown in this work.
4. Moreover, the performance does not degrade even for long simulation times.

4 Actuation and Controlled Motion

4.1 Motion Planning for Moving between Ground Locations

Consider a trajectory connecting two ground points with known initial and final velocities; there are many ways to generate this trajectory while avoiding fixed obstacles. The motion of the torso center of mass, when projected on the horizontal (ground) plane, should closely follow this generated trajectory. Assuming that this trajectory is known a priori, a stride length that is optimal (or natural) for the RMB is used to determine the number of steps required to cover the path length. If l_s is the optimal stride length and p_l is the path length of the trajectory, then the nearest integer to p_l/l_s can be used as the number of strides required to cover this trajectory.

Desired trajectories (motion primitives) for variables associated with the RMB legs in time interval $[0, T]$ are:

$$\begin{aligned} \rho_1^d &= \rho_0 + \bar{\rho}\sin(\omega t),\ \omega = \frac{\pi}{T},\ \rho_0 > \bar{\rho} > 0, \\ R_1^d &= R_{1_0} \exp\big(\zeta_1^\times \sin(\omega t/2)\big), \\ \rho_2^d &= \rho_0, \\ R_2^d &= R_{2_0} \exp\big(\zeta_2^\times \sin(\omega t/2)\big). \end{aligned} \tag{41}$$

Note that the constant vectors $\zeta_1, \zeta_2 \in \mathbb{R}^3$ for the leg rotations could be equal, and something similar could be said for $R_{1_0}, R_{2_0} \in \mathrm{SO}(3)$ when the biped is standing erect. Also, ρ_0 and $\bar{\rho}$ are related to the optimal stride length for the biped. The desired trajectories for variables associated with the torso over the time interval $[0, T]$ are:

$$\begin{aligned} R_P^d &= R_1^d \exp\Big(\gamma \log\big((R_1^d)^{\mathrm{T}} R_2^d\big)\Big),\ \gamma \in [0, 1], \\ s^d &= s_0 + \bar{s}\sin(\omega t), \end{aligned} \tag{42}$$

where $s_0, \bar{s} \in \mathbb{R}^3$ are designed to have the appropriate inertia distribution for the torso as mentioned earlier with $|s_{0i}| > |\bar{s}_i|$, $\log : \mathrm{SO}(3) \to \mathfrak{so}(3)$ is the logarithm map that is inverse of the exponential map (given by the matrix exponential), and γ is a weight factor. Note that $R_P^d = R_1^d$ when $\gamma = 0$ and $R_P^d = R_2^d$ when $\gamma = 1$. The reasoning behind introducing these weights is to mimic human bipedal gait, where the body (torso) becomes more closely aligned with the alignment of the stance leg as the speed of bipedal motion increases. By making γ and ω time-varying, one can even transition between different speeds of bipedal motion. This is one of the future goals of this research.

The stride length is given by the horizontal distance traversed by the ankle joint of the swing leg in one cycle. The desired stride length can be obtained from the above desired motions for the swing leg, considering that the inertial position of the ankle/foot of the swing leg at an instant is given by

$$a_{L2} = a_{L1} + \rho_1 R_1 e_3 - \rho_2 R_2 e_3, \tag{43}$$

where a_{L1}, a_{L2} denote the positions of the ankles of the stance and swing leg, respectively. With the coordinate frames as illustrated in Fig. 1 and substituting equation (41) for the desired motion trajectories, the starting and end positions of the swing leg ankle during a cycle are:

$$\begin{aligned} a_{L2}^s &= a_{L1} + \rho_0 R_{1_0} e_3 - \rho_0 R_{2_0} e_3, \\ a_{L2}^e &= a_{L1} + \rho_0 R_{1_0} \exp(\zeta_1^\times) e_3 - \rho_0 R_{2_0} \exp(\zeta_2^\times) e_3 \end{aligned} \tag{44}$$

Therefore the stride length is given by

$$a_{L2}^e - a_{L2}^s = \rho_0 R_{1_0}\big(\exp(\zeta_1^\times) - I\big)e_3 + \rho_0 R_{2_0}\big(I - \exp(\zeta_2^\times)\big)e_3. \tag{45}$$

Using Rodrigues' rotation formula, the above expression can be simplified to

$$\begin{aligned} v_s^d = \rho_0 R_{1_0} \big\{ \hat{\zeta}_1^\times \sin\|\zeta_1\| + \big(\hat{\zeta}_1^\times\big)^2 (1 - \cos\|\zeta_1\|) \big\} e_3 \\ - \rho_0 R_{2_0} \big\{ \hat{\zeta}_2^\times \sin\|\zeta_2\| + \big(\hat{\zeta}_2^\times\big)^2 (1 - \cos\|\zeta_1\|) \big\} e_3, \end{aligned} \tag{46}$$

where v_s^d denotes the desired stride vector, and $\hat{\zeta}_1, \hat{\zeta}_2$ denote the unit vectors along ζ_1, ζ_2 respectively. This sets the desired stride length to $l_s^d = \|v_s^d\|$. Note that the constraint $e_3^{\mathrm{T}} v_s^d = 0$ must be satisfied, which imposes certain constraints on R_{1_0}, R_{2_0}, ζ_1 and ζ_2. Substituting (46) for v_s^d, this constraint is expressed as

$$\begin{aligned} &\Gamma_{1_0}^{\mathrm{T}} \big\{ \hat{\zeta}_1^\times \sin\|\zeta_1\| + \big(\hat{\zeta}_1^\times\big)^2 (1 - \cos\|\zeta_1\|) \big\} e_3 = \\ &\Gamma_{2_0}^{\mathrm{T}} \big\{ \hat{\zeta}_2^\times \sin\|\zeta_2\| + \big(\hat{\zeta}_2^\times\big)^2 (1 - \cos\|\zeta_1\|) \big\} e_3, \\ &\text{where } \Gamma_{1_0} = R_{1_0}^{\mathrm{T}} e_3,\ \Gamma_{2_0} = R_{2_0}^{\mathrm{T}} e_3. \end{aligned} \tag{47}$$

Expression (47) can be satisfied by setting

$$\zeta_1 = \zeta_2 \text{ and } R_{2_0} = \exp(\theta e_3^\times) R_{1_0}, \tag{48}$$

for $\theta \in \mathbb{S}^1$. The second equality in (48) guarantees that $\Gamma_{1_0} = \Gamma_{2_0}$; physically, it means that the initial orientations of the stance and swing legs during start of a cycle are related by a rotation about the inertial third axis that points up. Substituting (48) in (42) to simplify the expression for R_P^d in (42), one obtains:

$$\begin{aligned} (R_1^d)^{\mathrm{T}} R_2^d &= \exp\big(-c(t)\zeta_1^\times\big) R_{1_0}^{\mathrm{T}} R_{2_0} \exp\big(c(t)\zeta_1^\times\big) \\ &= \exp\big(-c(t)\zeta_1^\times\big) \exp\big(\theta (R_{1_0}^{\mathrm{T}} e_3)^\times\big) \exp\big(c(t)\zeta_1^\times\big) \\ &= \exp\Big(\theta \big(\exp(-c(t)\zeta_1^\times) R_{1_0}^{\mathrm{T}} e_3\big)^\times\Big), \end{aligned} \tag{49}$$

where $c(t) = \sin(\omega t/2)$. The above simplification uses the following relation multiple times:

$$R^{\mathrm{T}} \exp(\phi e^\times) R = \exp\big(\phi (R^{\mathrm{T}} e)^\times\big),$$

where $e \in \mathbb{S}^2$ is a unit vector. This leads to the following simplified expression for R_P^d:

$$R_P^d = R_1^d \exp\Big(\gamma\theta \big(\exp(-c(t)\zeta_1^\times) R_{1_0}^{\mathrm{T}} e_3\big)^\times\Big), \tag{50}$$

which can then be expanded using Rodrigues' formula.

4.2 Trajectory Tracking Control Scheme

Define the trajectory tracking errors:

$$\begin{aligned}
&\tilde{\rho}_1 = \rho_1 - \rho_1^d, \quad \dot{\tilde{\rho}}_1 = \frac{\mathrm{d}}{\mathrm{d}t}\tilde{\rho}_1, \\
&Q_1 = R_1 (R_1^d)^{\mathrm{T}}, \quad \tilde{\Omega}_1 = \Omega_1 - \Omega_1^d, \\
&Q_P = R_P (R_P^d)^{\mathrm{T}}, \quad \tilde{\Omega}_P = \Omega_P - \Omega_P^d, \\
&\tilde{s} = s - s^d, \quad \dot{\tilde{s}} = \frac{\mathrm{d}}{\mathrm{d}t}\tilde{s}, \\
&Q_2 = R_2 (R_2^d)^{\mathrm{T}}, \quad \tilde{\Omega}_2 = \Omega_2 - \Omega_2^d.
\end{aligned} \tag{51}$$

The trajectory tracking control scheme is a generalization of the control scheme in [26]. The Lyapunov function candidate for the stance leg is:

$$\begin{aligned}
V_{L_1}(\rho_1, \tilde{\rho}_1, Q_1, \dot{\tilde{\rho}}_1, \tilde{\Omega}_1) = \frac{1}{2} m \dot{\tilde{\rho}}_1^2 + \frac{1}{2} \tilde{\Omega}_1^{\mathrm{T}} J_1(\rho_1) \tilde{\Omega}_1 + \frac{1}{2} k \tilde{\rho}_1^2 \\
+ \Phi\big(\mathrm{tr}(A - A Q_1)\big),
\end{aligned} \tag{52}$$

where $k > 0$, $A = \mathrm{diag}(a_1, a_2, a_3)$ with $a_1 > a_2 > a_3 > 0$, and $\Phi : \mathbb{R} \to \mathbb{R}$ is a $\mathcal{C}^2$ function that satisfies $\Phi(0) = 0$ and $\Phi'(x) > 0$ for all $x \in \mathbb{R}^+$. Furthermore, let $\Phi'(\cdot) \leq \alpha(\cdot)$, where $\alpha(\cdot)$ is a Class-$\mathcal{K}$ function [15]. The Lyapunov function candidate for the torso of the RMB is:

$$\begin{aligned}
V_P(Q_P, \tilde{\Omega}_P, s, \tilde{s}, \dot{\tilde{s}}) = \frac{1}{2} \tilde{\Omega}_P^{\mathrm{T}} J_P(s) \tilde{\Omega}_P + m_P \dot{\tilde{s}}^{\mathrm{T}} \dot{\tilde{s}} + \frac{1}{2} \tilde{s}^{\mathrm{T}} P \tilde{s} \\
+ \Phi\big(\mathrm{tr}(A - A Q_P)\big).
\end{aligned} \tag{53}$$

The Lyapunov function candidate for the swing leg is:

$$V_{L_2}(Q_2, \tilde{\Omega}_2) = \frac{1}{2} \tilde{\Omega}_2^{\mathrm{T}} J_{L_0} \tilde{\Omega}_2 + \Phi\big(\mathrm{tr}(A - A Q_2)\big), \tag{54}$$

where J_{L_0} is the inertia of swing leg at its nominal length (ρ_0), which is kept constant during swing phase, and P, Q_1, Q_P, Q_2 are suitable positive definite matrices that are use to build valid Lyapunov functions. The time derivative of these Lyapunov functions along the stance dynamics of the RMB system are evaluated next.

The time derivative of V_{L_1} along dynamics (11)-(12) is:

$$\begin{aligned}
&\frac{\mathrm{d}}{\mathrm{d}t} V_{L_1}(\rho_1, \tilde{\rho}_1, Q_1, \dot{\tilde{\rho}}_1, \tilde{\Omega}_1) = \dot{\tilde{\rho}}_1 \Big[f_1 - m \rho_1 \Omega_1^{\mathrm{T}} \big(e_3^{\times}\big)^2 \Omega_1 \\
&+ m g e_3^{\mathrm{T}} \Gamma_1 - m \ddot{\rho}_1^d + k \tilde{\rho}_1 \Big] \\
&+ \tilde{\Omega}_1^{\mathrm{T}} \Big[- \Omega_1 \times J_1(\rho_1) \Omega_1 + 2 m \rho_1 \dot{\rho}_1 \big(e_3^{\times}\big)^2 \Omega_1 + m g \rho_1 e_3^{\times} \Gamma_1 \\
&+ \tau_1 - R_1^{\mathrm{T}} R_P \tau_{D_1} - J_1(\rho_1) \dot{\Omega}_1^d - m \rho_1 \dot{\rho}_1 \big(e_3^{\times}\big)^2 \tilde{\Omega}_1 \\
&+ \Phi'\big(\mathrm{tr}(A - A Q_1)\big) (R_1^d)^{\mathrm{T}} S(Q_1) \Big],
\end{aligned} \tag{55}$$

where $\Gamma_1 = R_1^{\mathrm{T}} e_3$ is the inertial z-axis direction (upwards) in the stance leg's body-fixed frame and $S : \mathrm{SO}(3) \to \mathbb{R}^3$ is defined by

$$S(Q) = \sum_{i=1}^{3} a_i Q^{\mathrm{T}} e_i \times e_i. \tag{56}$$

After some partial cancellations of terms, this expression can be rewritten as

$$\begin{aligned}\frac{\mathrm{d}}{\mathrm{d}t} V_{L_1}(\rho_1, \tilde{\rho}_1, Q_1, \dot{\tilde{\rho}}_1, \tilde{\Omega}_1) &= \dot{\tilde{\rho}}_1 \Big[f_1 - m\ddot{\rho}_1^d - m\rho_1 \Omega_1 \big(e_3^{\times}\big)^2 \Omega_1 + mge_3^{\mathrm{T}} \Gamma_1 + k\tilde{\rho}_1 \Big] \\ &+ \tilde{\Omega}_1^{\mathrm{T}} \Big[\tau_1 - R_1^{\mathrm{T}} R_P \tau_{D_1} - \Omega_1^d \times J_1(\rho_1)\Omega_1 + m\rho_1 \dot{\rho}_1 \big(e_3^{\times}\big)^2 \big(\Omega_1 + \Omega_1^d\big) \\ &+ mg\rho_1 e_3^{\times} \Gamma_1 + \Phi'\big(\mathrm{tr}(A - AQ_1)\big)(R_1^d)^{\mathrm{T}} S(Q_1) \Big]. \end{aligned} \tag{57}$$

The time derivative of V_P along the dynamics (13)-(14) is:

$$\begin{aligned}\frac{\mathrm{d}}{\mathrm{d}t} V_P(Q_P, \tilde{\Omega}_P, s, \tilde{s}, \dot{\tilde{s}}) &= \tilde{\Omega}_P^{\mathrm{T}} \Big[J_P(s)\Omega_P \times \Omega_P + \tau_{D_1} - N(s, \dot{s})\Omega_P - R_P^{\mathrm{T}} R_2 \tau_{D_2} \\ &- J_P(s)\dot{\Omega}_P^d + \frac{1}{2} N(s, \dot{s})\tilde{\Omega}_P + \Phi'\big(\mathrm{tr}(A - AQ_P)\big)(R_P^d)^{\mathrm{T}} S(Q_P) \Big] \\ &+ \dot{\tilde{s}}^{\mathrm{T}} \Big[L(s, \Omega_P) - 2m_P \ddot{s}^d + P\tilde{s} + u_s \Big], \end{aligned} \tag{58}$$

where $N(s, \dot{s}) = \frac{\mathrm{d}}{\mathrm{d}t} K_P(s)$ and $\dot{s}^{\mathrm{T}} L(s, \Omega_P) = \frac{1}{2} \Omega_P^{\mathrm{T}} N(s, \dot{s}) \Omega_P$. After some partial cancellation of terms, one can simplify expression (58) to

$$\begin{aligned}\frac{\mathrm{d}}{\mathrm{d}t} V_P(Q_P, \tilde{\Omega}_P, s, \tilde{s}, \dot{\tilde{s}}) &= \tilde{\Omega}_P^{\mathrm{T}} \Big[\tau_{D_1} - R_P^{\mathrm{T}} R_2 \tau_{D_2} - J_P(s)\dot{\Omega}_P^d - \Omega_P^d \times J_P(s)\Omega_P \\ &- \frac{1}{2} N(s, \dot{s})\big(\Omega_P + \Omega_P^d\big) + \Phi'\big(\mathrm{tr}(A - AQ_P)\big)(R_P^d)^{\mathrm{T}} S(Q_P) \Big] \\ &+ \dot{\tilde{s}}^{\mathrm{T}} \Big[u_s + L(s, \Omega_P) - 2m_P \ddot{s}^d + P\tilde{s} \Big]. \end{aligned} \tag{59}$$

Finally, the time derivative of V_{L_2} along dynamics (15) is

$$\begin{aligned}\frac{\mathrm{d}}{\mathrm{d}t} V_{L_2}(Q_2, \tilde{\Omega}_2) = \frac{1}{2} \tilde{\Omega}_2^{\mathrm{T}} \Big(&- \Omega_2^d \times J_{L_0} \Omega_2 + \tau_{D_2} - J_{L_0} \dot{\Omega}_2^d \\ &+ \Phi'\big(\mathrm{tr}(A - AQ_2)\big)(R_2^d)^{\mathrm{T}} S(Q_2) \Big). \end{aligned} \tag{60}$$

Theorem 1 *Let $\ell > 0$ and let $D_1, D_P, D_2, P, Q \in \mathbb{R}^{3\times 3}$ be positive definite matrices. Then the tracking control laws*

$$f_1 = m\ddot{\rho}_1^d + m\rho_1 \Omega_1^T \big(e_3^{\times}\big)^2 \Omega_1 - mge_3^T \Gamma_1 - k\tilde{\rho}_1 - \ell\dot{\tilde{\rho}}_1, \tag{61}$$

$$\begin{aligned}\tau_1 = R_1^T R_P \tau_{D_1} + J_1(\rho_1)\dot{\Omega}_1^d + \Omega_1^d \times J_1(\rho_1)\Omega_1 - mg\rho_1 e_3^{\times} \Gamma_1 \\ - m\rho_1 \dot{\rho}_1 \big(e_3^{\times}\big)^2 \big(\Omega_1 + \Omega_1^d\big) - \Phi'\big(tr(A - AQ_1)\big)(R_1^d)^T S(Q_1) - D_1 \tilde{\Omega}_1, \end{aligned} \tag{62}$$

$$\begin{aligned}\tau_{D_1} = R_P^T R_2 \tau_{D_2} + \Omega_P^d \times J_P(s)\Omega_P + J_P(s)\dot{\Omega}_P^d - D_P \tilde{\Omega}_P \\ + \frac{1}{2} N(s, \dot{s})\big(\Omega_P + \Omega_P^d\big) - \Phi'\big(tr(A - AQ_P)\big)(R_P^d)^T S(Q_P), \end{aligned} \tag{63}$$

$$u_s = 2m_P \ddot{s}^d - L(s, \Omega_P) - P\tilde{s} - Q\dot{\tilde{s}}, \tag{64}$$

$$\tau_{D_2} = \Omega_2^d \times J_{L_0} \Omega_2 + J_{L_0} \dot{\Omega}_2^d - D_2 \tilde{\Omega}_2 - \Phi'\big(tr(A - AQ_2)\big)(R_2^d)^T S(Q_2), \tag{65}$$

asymptotically stabilize a desired state trajectory of the form given by equations (41)-(42). Further, the domain of convergence of this trajectory is almost global in the state space in the absence of control constraints, disturbance forces and disturbance torques.

Proof. See Appendix A. □

Note that, this trajectory tracking control scheme can be applied in general to track all $\mathcal{C}^2$ desired state trajectories, provided that actuator constraints are not violated. In practice, the desired state trajectories can be designed keeping in mind known actuator constraints for the RMB or for a humanoid robot being modeled by the RMB.

5 Numerical Results

Having developed a geometric controller for asymptotically tracking trajectories, we now validate the proposed controller through a numerical simulation of the hybrid model developed in Section 2.

To illustrate the capability of the controller, we will demonstrate (a) walking in a straight line, (b) walking towards a goal location, and (c) walking in a circle. In all cases, we choose a constant desired torso angle leaning forward, this is in contrast to (42) to simplify velocity and acceleration computation. The mass and inertia properties of the reaction mass biped are chosen to be similar to that of a NAO robot, as done in [26], in particular,

$$m_L = 0.882\text{kg}, J_{L_0} = 0.5 diag\{0.98, 0.91, 0.63\}\text{kg-m}^2,$$
$$m_P = 0.32\text{kg}, J_{P_0} = \begin{bmatrix} 0.2126 & 0.0004 & -0.0002 \\ 0.0004 & 0.2042 & 0.0010 \\ -0.0002 & 0.0010 & 0.2246 \end{bmatrix} \text{kg-m}^2.$$

Motion Primitive Parameters
$\rho_0 = 0.9, \quad \bar{\rho} = 0.1, \quad s = 0.125, \quad \bar{s} = 0.025.$
Controller Tuning Parameters
$\epsilon = 0.25, \quad k = \frac{16}{\epsilon^2}, \quad l = \frac{8}{\epsilon}, \quad A = \frac{1}{\epsilon^2}\text{diag}(1.2, 1.5, 1.8), \quad L = (1.5)(1.2)\text{diag}(1,1,1),$
$D1 = \frac{2}{\epsilon}\text{diag}(1,1,1), \quad D2 = \frac{0.5}{\epsilon}\text{diag}(1,1,1), \quad P = \frac{1.2}{\epsilon^2}\text{diag}(1,1,1), \quad Q = \frac{1.5}{\epsilon}\text{diag}(1,1,1).$

Table 3: List of various tuning parameters used in the Motion Primitive and Controller designs.

Walking in a straight line: We chose $\zeta_1 = \zeta_2 = e_2, R_{10} = R_{20} = I$, and $T = 1$s as in (41). Moreover, we introduce a constant phase offset in the angles for R_1^d, R_2^d to enable the swing legs to swing from -15° to 15°. For all other motion design and controller gain parameters, see Table 3. Figure 3a illustrates a snapshot and the tracking errors.

Walking towards a goal: We employ the walking in a straight line controller as above, however, we perform an event-based modification of R_{10}, R_{20} at each

impact to change the heading of the biped. Figure 3b illustrates a snapshot and the tracking errors. Note that at each impact, the desired yaw instantaneously changes and the controller is able to regulate the errors asymptotically within a step.

Walking in a circle: We employ the walking towards a goal controller as above, however we modify R_{10}, R_{20} by a fixed amount at each impact. Moreover, R_{10}, R_{20} are also chosen to lean the body into the turn. Figure 3c illustrates a snapshot (along with the hip position demonstrating the body lean) and the tracking errors. Note that instead of modifying R_{10}, R_{20}, we could have modified ζ_1, ζ_2 too.

For all these motions, it is important to verify that the unilateral ground contact constraints and the friction constraints are satisfied during the walking, i.e., we need to ensure $|F_x| \leq \mu F_z$ and $|F_y| \leq \mu F_z$, where μ is the coefficient of static friction. The ground reaction forces were computed as, $\mathbf{F}_G = m\ddot{x}_{cm} - mge_3$, where $\mathbf{F}_G := [F_x\ F_y\ F_z]$ and x_{cm} is the center-of-mass of the RMB. It is equally critical to verify these constraints for the impact forces (I_R in Section 2.3) generated at the end of every step. Note that, the above-mentioned three motions namely a) 'walking in a straight line', b) 'walking towards a goal' and c) 'walking in a circle', take 10, 13, 19 steps respectively. In all these impact situations, we note that I_{R_z} is always positive ($\geq 1.6019\ N$). Moreover, the maximum values of $\frac{|I_{R_x}|}{I_{R_z}}$ and $\frac{|I_{R_y}|}{I_{R_z}}$ are 0.5872 and 0.5888, respectively, both occurring while walking in a circle.

Combining the impact-force data with the stance leg ground reaction force information, as shown in the third row of Fig. 3a, 3b, 3c, we can conclude that, for $\mu \geq 0.6$, the ground reaction force and the impact force respect the unilateral and friction cone constraints, thereby validating the assumptions that 1) stance leg is pinned to the ground during stance-phase and 2) No slip occurs at impact.

In addition to testing the trajectory tracking controller on the continuous-time dynamics model of the RMB, it was also tested on the Discrete-time model developed in Section 3. Figure 4 shows the performance of the GVI in comparison to the traditional Runge-Kutta(4,5)-based integrator (RK45). RK45 is a very popular numerical integration algorithm based on the explicit Runge-Kutta formula [3]. It is also part of Matlab's ODE suite [27].

In Fig. 4(a), the two integrators are compared for a two-step walking scenario where the robot is initialized along the desired nominal trajectory(here, we chose the 'walking in a circle' trajectory) given by (41) and (42): $q_{s_0} = (\rho_0, R_{1_0}, R_{P_0}, s_0, R_{2_0})$. On the other hand, in 4(b), we start with a perturbed initial conditions: $q_{s_0}^{pert} = (\rho_0 + 0.1, R_x(\pi/10)R_{1_0}, R_{P_0}, s_0, R_{2_0})$ and $\omega_{s_0}^{pert} = (\dot{\rho}_0, \Omega_{1_0}, \Omega_{P_0} + 0.01, \dot{s}_0 - 0.03, \Omega_{2_0})$. Here $R_x(\theta)$ denotes a rotation along the x-direction by an angle θ. For both these cases, we plot (a) the desired leg extension tracking error ($\bar{\rho}$) as obtained from (51) , (b) discrete Lyapunov function (obtained by discretizing (52), (53) and (54)) given by (66), and (c)-(d) R_1, R_2 norm errors. The norm errors are computed as $||I - R_i^T R_i|| \quad \forall i \in \{1, 2\}$. If the group structure ($R \in \mathbb{SO}(3)$) of R_1 and R_2 is preserved during the numerical

integrations, the norm errors must be closer to zero.

$$V_k(\tilde{\rho}_{1_k}, Q_{1_k}, \dot{\tilde{\rho}}_{1_k}, \tilde{\Omega}_{1_k}, Q_{P_k}, \Omega_{P_k}, \tilde{s}_k, \dot{\tilde{s}}_k, Q_{2_k}, \tilde{\Omega}_{2_k}) = V_{L_{1_k}}(\rho_{1_k}, \tilde{\rho}_{1_k}, Q_{1_k}, \dot{\tilde{\rho}}_{1_k}, \tilde{\Omega}_{1_k}) + V_{P_k}(Q_{P_k}, \tilde{\Omega}_{P_k}, s_k, \tilde{s}_k, \dot{\tilde{s}}_k) + V_{L_{2_k}}(Q_{2_k}, \tilde{\Omega}_{2_k}) \quad (66)$$

where,

$$\begin{aligned} V_{L_{1_k}}(\rho_{1_k}, \tilde{\rho}_{1_k}, Q_{1_k}, \dot{\tilde{\rho}}_{1_k}, \tilde{\Omega}_{1_k}) &= \frac{1}{2} m \dot{\tilde{\rho}}_{1_k}^2 + \frac{1}{2} \tilde{\Omega}_{1_k}^{\mathrm{T}} J_1(\rho_{1_k}) \tilde{\Omega}_{1_k} + \frac{1}{2} k \tilde{\rho}_{1_k}^2 \\ &\quad + \Phi\big(\mathrm{tr}(A - AQ_{1_k})\big), \\ V_{P_k}(Q_{P_k}, \tilde{\Omega}_{P_k}, s_k, \tilde{s}_k, \dot{\tilde{s}}_k) &= \frac{1}{2} \tilde{\Omega}_{P_k}^{\mathrm{T}} J_P(s_k) \tilde{\Omega}_{P_k} + m_P \dot{\tilde{s}}_k^{\mathrm{T}} \dot{\tilde{s}}_k + \frac{1}{2} \tilde{s}_k^{\mathrm{T}} P \tilde{s}_k \\ &\quad + \Phi\big(\mathrm{tr}(A - AQ_{P_k})\big), \\ V_{L_{2_k}}(Q_{2_k}, \tilde{\Omega}_{2_k}) &= \frac{1}{2} \tilde{\Omega}_{2_k}^{\mathrm{T}} J_{L_0} \tilde{\Omega}_{2_k} + \Phi\big(\mathrm{tr}(A - AQ_{2_k})\big). \end{aligned} \quad (67)$$

Note that, for this study the step size chosen for the GVI and RK45 was $h = 10^{-3}$. From the third and fourth rows of Fig.4, it is can be noted that the variational integrator maintained the group structure much better than the RK45 Integrator. On further examination, it was found that the GVI kept the norm error within 10^{-12} which is orders of magnitude better than RK45. Moreover, other parameters like configuration errors($\bar{\rho}$), energies, etc., as computed using the discrete GVI-based system model, track the continuous dynamics as accurately as the discrete-model based on RK45, if not better.

6 Conclusion and Future Work

A variable inertia multi-body reduced-order reaction mass biped model (RMB) is presented that can capture a much wider class of bipedal locomotion. A coordinate-free hybrid dynamical model of the RMB is developed. A discrete version of the model has also been developed that maintains the structural and geometrical properties of the system and enables fast implementations on hardware. An asymptotically stable trajectory tracking control scheme with almost global domain of convergence was also developed to enable the reaction mass biped to walk along straight and curved paths.

Despite all the useful additions, the RMB has room for improvement. The influence of the reaction masses and the varying torso inertia on the gait design is not investigated. The primary objective of future work is to study the impact of upper-body inertia on RMB's locomotory behavior. Additionally, the proof masses are constrained to move together, either towards or away from each other. We assume full actuation, but in reality there are under-actuated phases (toe-off) in walking which are not captured by this model. These constraints will be relaxed in future works. Finally, the center-of-mass is assumed to be at the hip. This makes the dynamics of the torso, swing and stance legs fully decoupled thereby simplifying the control design.

As a part of future work, a variational collision integrator [23] needs to be added to the discrete dynamics to complete the discrete hybrid model for walking. Finally, optimization and optimal control policy for walking and turning can be developed. Ultimately, the objective of the RMB is to achieve a wider variety of gaits, like high-lean turning, running, dynamic balancing, etc. After having developed sufficient mathematical machinery that lead to the discovery of efficient and stable walking gaits for the coordinate-free RMB model, our final goal is to validate our results on an appropriate 3D bipedal robot in the near future.

Appendix

A Theorem 1 Proof:

Consider the Lyapunov function

$$V(\tilde{\rho}_1, Q_1, \dot{\tilde{\rho}}_1, \tilde{\Omega}_1, Q_P, \Omega_P, s, \dot{s}, Q_2, \tilde{\Omega}_2) = V_{L_1}(\rho_1, \tilde{\rho}_1, Q_1, \dot{\tilde{\rho}}_1, \tilde{\Omega}_1) + V_P(Q_P, \tilde{\Omega}_P, s, \tilde{s}, \dot{\tilde{s}}) + V_{L_2}(Q_2, \tilde{\Omega}_2), \tag{68}$$

which captures the three coupled components: the stance leg, torso, and swing leg, of the RMB. The time derivative of this Lyapunov function is obtained by substituting expressions (69), (70) and (71) for the time derivatives of V_{L_1}, V_P, and V_{L_2} respectively. Further substitutions of the control laws (61)-(65) in these expressions gives the time derivatives along trajectories of the feedback tracking system

$$\dot{V}_{L_1}(\dot{\tilde{\rho}}_1, \tilde{\Omega}_1) = -\ell \dot{\tilde{\rho}}_1^2 - \tilde{\Omega}_1^{\mathrm{T}} L_1 \tilde{\Omega}_1, \tag{69}$$

$$\dot{V}_P(\tilde{\Omega}_P, \dot{\tilde{s}}) = -\tilde{\Omega}_P^{\mathrm{T}} L_P \tilde{\Omega}_P - \dot{\tilde{s}}^{\mathrm{T}} Q \dot{\tilde{s}}, \tag{70}$$

$$\dot{V}_{L_2}(\tilde{\Omega}_2) = -\tilde{\Omega}_2^{\mathrm{T}} L_2 \tilde{\Omega}_2. \tag{71}$$

This makes the time derivative of the overall Lyapunov function negative semi-definite:

$$\dot{V}(\dot{\tilde{\rho}}_1, \tilde{\Omega}_1, \tilde{\Omega}_P, \dot{\tilde{s}}, \tilde{\Omega}_2) = -\ell \dot{\tilde{\rho}}_1^2 - \tilde{\Omega}_1^{\mathrm{T}} L_1 \tilde{\Omega}_1 - \tilde{\Omega}_P^{\mathrm{T}} L_P \tilde{\Omega}_P - \dot{\tilde{s}}^{\mathrm{T}} Q \dot{\tilde{s}} - \tilde{\Omega}_2^{\mathrm{T}} L_2 \tilde{\Omega}_2. \tag{72}$$

Assuming that the desired motion trajectories are bounded and continuous, as is the case with the desired motions given by (41)-(42), then V as given by (68) is positive definite and is bounded above and below by suitably chosen positive definite functions of the trajectory tracking error states. Therefore, invoking invariance-like principle given by Theorem 8.4 in [15], one can conclude that $\dot{V}$ converges asymptotically to zero. Therefore, the positive limit set for the feedback tracking control system is a subset of

$$\dot{V}^{-1}(0) = \big\{(\tilde{\rho}_1, Q_1, \dot{\tilde{\rho}}_1, \tilde{\Omega}_1, Q_P, \Omega_P, \dot{\tilde{s}}, Q_2, \tilde{\Omega}_2) \,:\, \dot{\tilde{\rho}}_1 = 0, \; \tilde{\Omega}_1 = 0,\, \tilde{\Omega}_P = 0,\, \dot{\tilde{s}} = 0,\, \tilde{\Omega}_2 = 0\big\}. \tag{73}$$

The feedback dynamics can be expressed in terms of the tracking errors as follows:

$$m\ddot{\tilde{\rho}}_1 = -\ell \dot{\tilde{\rho}}_1 - k\tilde{\rho}_1, \tag{74}$$

$$J_1(\rho_1)\dot{\tilde{\Omega}}_1 = -\tilde{\Omega}_1 \times J_1(\rho_1)\Omega_1 + m\rho_1\dot{\rho}_1\big(e_3^{\times}\big)^2\tilde{\Omega}_1 - D_1\tilde{\Omega}_1 - \Phi'\big(\mathrm{tr}(A - AQ_1)\big)(R_1^d)^{\mathrm{T}} S(Q_1), \tag{75}$$

$$J_P(s)\dot{\tilde{\Omega}}_P = -\tilde{\Omega}_P \times J_P(s)\Omega_P - \frac{1}{2}N(s,\dot{s})\tilde{\Omega}_P - D_P\tilde{\Omega}_P - \Phi'\big(\mathrm{tr}(A - AQ_P)\big)(R_P^d)^{\mathrm{T}} S(Q_P), \tag{76}$$

$$2m_P\ddot{\tilde{s}} = -Q\dot{\tilde{s}} - P\tilde{s}, \tag{77}$$

$$J_{L_0}\dot{\tilde{\Omega}}_2 = -\tilde{\Omega}_2 \times J_{L_0}\Omega_2 - D_2\tilde{\Omega}_2 - \Phi'\big(\mathrm{tr}(A - AQ_2)\big)(R_2^d)^{\mathrm{T}} S(Q_2). \tag{78}$$

Therefore in the set $\dot{V}^{-1}(0)$, the feedback dynamics is restricted to

$$\tilde{\rho}_1 = 0,\ \Phi'\big(\mathrm{tr}(A - AQ_1)\big) = 0,\ \Phi'\big(\mathrm{tr}(A - AQ_P)\big) = 0,$$
$$\tilde{s} = 0, \text{ and } \Phi'\big(\mathrm{tr}(A - AQ_2)\big) = 0, \tag{79}$$

which characterizes the positive limit set of the feedback tracking system. Note that within the set of four critical points $\mathcal{E}_c$ of $\Phi\big(\mathrm{tr}(A - AQ)\big)$, it can be shown, as in [24,25,2], that $Q = I$ is the minimum, while the other points ($Q \in \mathcal{E}_c \setminus I$) are non-degenerate critical points. Therefore, as $\dot{V} \leq 0$ along the trajectories of the feedback system, the only stable subset of the positive limit set is when the actual motion is tracking the desired motion, i.e.,

$$\tilde{\rho}_1 = 0,\ Q_1 = I,\ Q_P = I,\ \tilde{s} = 0, \text{ and } Q_2 = I. \tag{80}$$

The other subsets (corresponding to $Q_1, Q_P, Q_2 \in \mathcal{E}_c \setminus I$) are unstable, although they may have stable subsets. Except for trajectories that start on these stable subsets of the positive limit set, all other trajectories in the state space converge asymptotically to the desired state trajectory. This means that the set $\mathcal{S}_L$ is asymptotically stable and its domain of attraction is almost-global.

References

1. R. Altendorfer, U. Saranli, H. Komsuoglu, D. Koditschek, H. B. Brown, M. Buehler, N. Moore, D. McMordie, and R. Full, "Evidence for spring loaded inverted pendulum running in a hexapod robot," in *Experimental Robotics VII*, D. Rus and S. Singh, Eds. Springer-Verlag, 2001, pp. 291 – 302.
2. N. A. Chaturvedi, A. K. Sanyal, and N. H. McClamroch, "Rigid-Body Attitude Control: Using rotation matrices for continuous, singularity-free control laws," *IEEE Control Systems Magazine*, vol. 31, no. 3, pp. 30–51, June 2011.
3. J. R. Dormand and P. J. Prince, "A family of embedded runge-kutta formulae," *Journal of computational and applied mathematics*, vol. 6, no. 1, pp. 19–26, 1980.
4. A. Dutta and A. Goswami, "Human postural model that captures rotational inertia," in *American Society of Biomechanics*, 2010.
5. H. Geyer, A. Seyfarth, and R. Blickhan, "Compliant leg behaviour explains basic dynamics of walking and running," *Proceedings of the Royal Society of London B: Biological Sciences*, vol. 273, no. 1603, pp. 2861–2867, 2006.
6. R. Gregg, A. Tilton, S. Candido, T. Bretl, and M. Spong, "Control and planning of 3d dynamic walking with asymptotically stable gait primitives," *IEEE Transactions on Robotics*, vol. 28, no. 6, pp. 1415–1423, 2012.
7. R. D. Gregg and M. W. Spong, "Reduction-based control of three-dimensional bipedal walking robots," *The International Journal of Robotics Research*, vol. 29, no. 6, pp. 680–702, May 2010.
8. J. W. Grizzle, C. Chevallereau, A. Ames, and R. Sinnet, "3d bipedal robotic walking: Models, feedback control, and open problems," in *IFAC Symposium on Nonlinear Control Systems*, Bologna, Italy, September 2010.
9. K. A. Hamed, B. G. Buss, and J. W. Grizzle, "Continous-time controllers for stabilizing periodic orbits of hybrid systems: application to an underactuated 3d bipedal robot," in *IEEE Conference on Decision and Control*, December 2014.
10. Y. Hürmüzlü and T. Chang, "Rigid body collisions of a special class of planar kinematic chains," *IEEE Transactions on Systems, Man and Cybernetics*, vol. 22, no. 5, pp. 964–71, 1992.
11. A. Iserles, H. Z. Munthe-Kaas, S. P. Nørsett, and A. Zanna, "Lie-group methods," *Acta Numerica 2000*, vol. 9, pp. 215–365, 2000.
12. S. Kajita, F. Kanehiro, K. Kaneko, K. Fujiwara, K. Harada, K. Yokoi, and H. Hirukawa, "Biped walking pattern generation by using preview control of zero-moment point," in *IEEE International Conference on Robotics and Automation (ICRA)*, 2003, Taipei, Taiwan, pp. 1620–1626.
13. S. Kajita, F. Kanehiro, K. Kaneko, K. Yokoi, and H. Hirukawa, "The 3D linear inverted pendulum model: A simple modeling for a biped walking pattern generator," in *IEEE/RSJ International Conference on Intelligent Robots and Systems (IROS)*, 2001, Maui, Hawaii, pp. 239–246.
14. S. Kajita and K. Tani, "Study of dynamic biped locomotion on rugged terrain," in *IEEE International Conference on Robotics and Automation (ICRA)*, 1991, pp. 1405–1411.
15. H. K. Khalil, *Nonlinear Systems*, 3rd ed. Englewood Cliffs, NJ: Prentice Hall, 2002.
16. M. Kobilarov, K. Crane, and M. Desbrun, "Lie group integrators for animation and control of vehicles," *ACM Transactions on Graphics (TOG)*, vol. 28, no. 2, p. 16, 2009.

17. T. Komura, H. Leung, S. Kudoh, and J. Kuffner, "A feedback controller for biped humanoids that can counteract large perturbations during gait," in *IEEE International Conference on Robotics and Automation (ICRA)*, 2005, Barcelona, Spain, pp. 2001–2007.
18. T. Komura, A. Nagano, H. Leung, and Y. Shinagawa, "Simulating pathological gait using the enhanced linear inverted pendulum model," *IEEE Transactions on Biomedical Engineering*, vol. 52, no. 9, pp. 1502–1513, 2005, September.
19. S.-H. Lee and A. Goswami, "Reaction mass pendulum (RMP): An explicit model for centroidal angular momentum of humanoid robots," in *IEEE International Conference on Robotics and Automation (ICRA)*, April 2007, Rome, Italy, pp. 4667–4672.
20. T. Lee, *Computational geometric mechanics and control of rigid bodies*. ProQuest, 2008.
21. T. Lee, N. H. McClamroch, and M. Leok, "A lie group variational integrator for the attitude dynamics of a rigid body with applications to the 3d pendulum," in *IEEE Conference on Control Applications (CCA)*. IEEE, 2005, pp. 962–967.
22. J. E. Marsden and M. West, "Discrete mechanics and variational integrators," *Acta Numerica 2001*, vol. 10, pp. 357–514, 2001.
23. D. N. Pekarek and J. E. Marsden, "Variational collision integrators and optimal control," 2008.
24. A. K. Sanyal and N. A. Chaturvedi, "Almost global robust attitude tracking control of spacecraft in gravity," in *AIAA Guidance, Navigation and Control Conference*, Aug 2008, Honolulu, pp. AIAA–2008–6979.
25. A. K. Sanyal, A. Fosbury, N. A. Chaturvedi, and D. S. Bernstein, "Inertia-free spacecraft attitude trajectory tracking with disturbance rejection and almost global stabilization," *AIAA Journal of Guidance, Control and Dynamics*, vol. 32, no. 2, pp. 1167–1178, Feb 2009.
26. A. K. Sanyal and A. Goswami, "Dynamics and balance control of the reaction mass pendulum (rmp): A 3d multibody pendulum with variable body inertia," *ASME Journal of Dynamic Systems, Measurement and Control*, vol. 136, no. 2, p. paper 021002, 2014.
27. L. F. Shampine and M. W. Reichelt, "The matlab ode suite," *SIAM journal on scientific computing*, vol. 18, no. 1, pp. 1–22, 1997.
28. C.-L. Shih, J. W. Grizzle, and C. Chevallereau, "From stable walking to steering of a 3d bipedal robot with passive point feet," *Robotica*, vol. 30, no. 7, pp. 1119–1130, 2012.
29. R. Sinnet and A. D. Ames, "3d bipedal walking with knees and feet: A hybrid geometric approach," in *IEEE Conference on Decision and Control*, December 2009, pp. 3208–3213.
30. K. Sreenath and A. K. Sanyal, "The reaction mass biped: Equations of motion, hybrid model for walking and trajectory tracking control," in *IEEE International Conference on Robotics and Automation (ICRA)*, 2015.
31. T. Sugihara and Y. Nakamura, "Variable impedance inverted pendulum model control for a seamless contact phase transition on humanoid robot," in *IEEE International Conference on Humanoid Robots (Humanoids2003)*, Oct 2003, Germany, pp. 0–0.
32. S. P. Viswanathan, A. K. Sanyal, F. Leve, and N. H. McClamroch, "Dynamics and control of spacecraft with a generalized model of variable speed control moment gyroscopes," *Journal of Dynamic Systems, Measurement, and Control*, vol. 137, no. 7, p. 071003, 2015.
33. M. West, "Variational integrators," Ph.D. dissertation, California Institute of Technology, 2004.

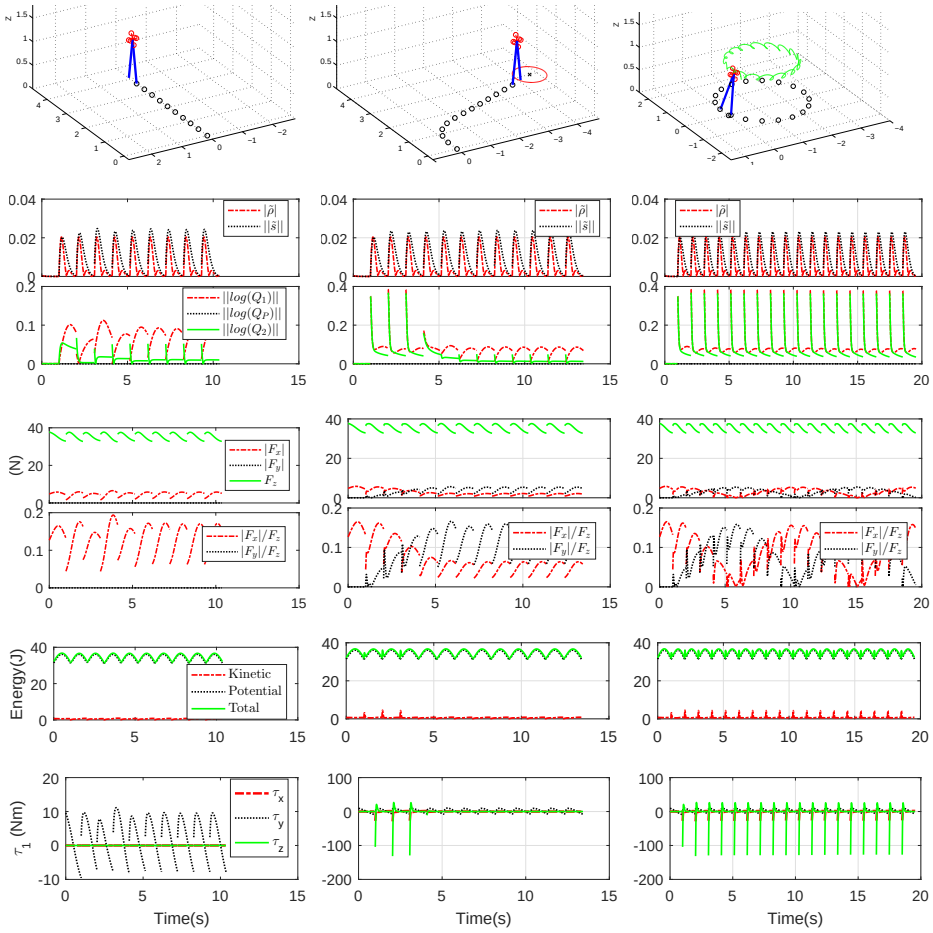

(a) Walking Straight (b) Walking to a Goal (c) Walking in a Circle

Fig. 3: Numerical simulations of the controller for (a) Walking along a straight line, (b) Walking towards a goal location by changing the yaw-angle in an event-based step-to-step manner, and (c) Walking in a circle while leaning inwards, with the hip position shown in green. For all these cases, first row shows simulation snapshots. The second row shows error plots to study controller behavior. The errors include those defined in (51), namely $|\tilde{\rho}_1|$, $||\tilde{s}||$, $||\log(Q_1)||$, $||\log(Q_P)||$, and $||\log(Q_2)||$. As can be seen, the controller reduces the error during the continuous stance-phase, while the impacts causes the errors to increase. The simulation begins with zero initial errors, and hence the errors during the first step remain zero. Third row shows ground reaction force plots and force-ratios. Note that, if you assume the coefficient of static friction to be greater than 0.6, RMB satisfies the no slip condition at the stance leg for all the three walking trajectories. Since the legs make a point contact with the ground, we can assume the friction forces (F_x and F_y) to be isotropic. Clearly, $\frac{|F_x|}{F_z} \leq 0.6$ and $\frac{|F_y|}{F_z} \leq 0.6$. Fourth row shows the energy plots for the closed-loop dynamics of the RMB walking. Finally, in the the fifth row, we show the ankle torque (τ_1) generated for the three walking trajectories. The x-axis for all the plots is Time(in seconds) and it is only shown for the fifth row to avoid repetitions.

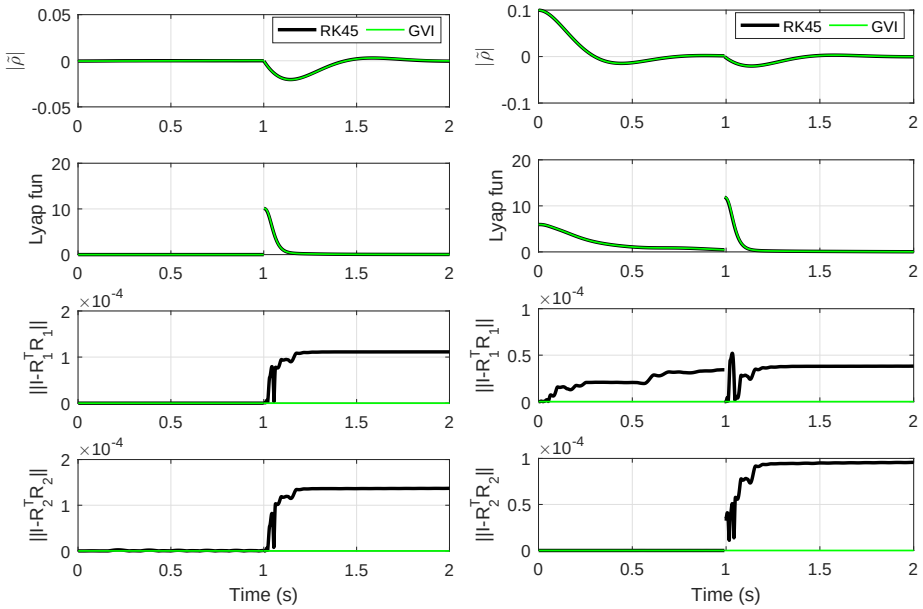

(a) Starting from desired configuration (b) Starting with some configuration error

Fig. 4: Comparing the performance of GVI with Runge-Kutta 45 based Integrator. In (a) RMB starts along the desired walking trajectory and a nominal controller is in action for tracking purposes. However, in (b), RMB starts with an initial error in its configuration.